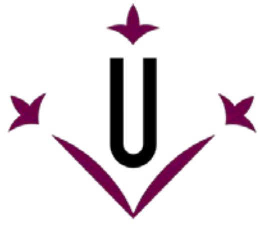

Document downloaded from:

http://hdl.handle.net/10459.1/65392

The final publication is available at:

https://doi.org/10.1016/j.bcp.2018.08.005

Copyright

cc-by-nc-nd, (c) Elsevier, 2018

Està subjecte a una llicència de Reconeixement-NoComercial-SenseObraDerivada 4.0 de Creative Commons

1 **TITLE PAGE**

2 **Pharmacological blockade of fatty acid amide hydrolase (FAAH) by URB597 improves**
3 **memory and induces changes in microglial morphology and phenotype related to innate**
4 **immune TLR4 system in the hippocampus despite ethanol exposure**

5

6 **Running title:** Cannabinoids in memory and neuroinflammation

7 **Categories:** Neuropharmacology and inflammation

8 Patricia Rivera[1,2], María del Mar Fernández-Arjona[3], Daniel Silva-Peña[1], Eduardo Blanco[4],
9 Antonio Vargas[1], María Dolores López-Ávalos[3], Jesús Mateos Grondona[3], Antonia Serrano[1],
10 Francisco Javier Pavón[1], Fernando Rodríguez de Fonseca[1,*], Juan Suárez[1,*]

11

12 *[1]UGC Salud Mental, Instituto de Investigación Biomédica de Málaga (IBIMA), Universidad*
13 *de Málaga, Hospital Universitario Regional de Málaga, Málaga, Spain. [2]Department of*
14 *Endocrinology, Fundación Investigación Biomédica del Hospital Infantil Universitario Niño*
15 *Jesús, Madrid, Spain. [3]Departamento de Biología Celular, Genética y Fisiología, IBIMA,*
16 *Universidad de Málaga, Málaga, Spain. [4]Institute of Biomedical Research of Lleida (IRB*
17 *Lleida), Universitat de Lleida, Lleida, Spain.*

18 ***Address for correspondence:**
19 Juan Suárez, e-mail: juan.suarez@ibima.eu
20 Fernando Rodríguez de Fonseca, e-mail: fernando.rodrigiez@ibima.eu
21 Laboratorio de Investigación. IBIMA. Hospital Universitario Regional de Málaga. Avenida
22 Carlos Haya 82, 29010 Málaga, Spain. Tel/fax number: +34952614012.

23

24 **FUNDING**

Instituto de Salud Carlos III (ISCIII), Ministerio de Economía y Competitividad (MINECO) co-funded by UE-ERDF program (JS: PI16/01374; FRF: PI16/01698); Ministerio de Sanidad, Servicios Sociales e Igualdad and Plan Nacional sobre Drogas (JS: PNSD2015/047); Consejería de Economía, Innovación y Ciencia, Junta de Andalucía, UE-ERDF (FRF: CTS-8221); Consejería de Salud, Junta de Andalucía, UE-ERDF (FRF: SAS111224). FJP (CP14/00212) and AS (CP14/00173) are recipients of a research contract from "Miguel Servet" Program of ISCIII, EU-ERDF. JS holds a "Miguel Servet II" research contract from the National System of Health, ISCIII, EU-ERDF, FIMABIS (CPII17/00024). PR holds a "Sara Borrel" research contract from ISCIII, EU-ERDF (CD16/00067).

AUTHOR CONTRIBUTIONS

The authors have declared that no competing interest exists. All authors had full access to all the data in the study and take responsibility for the integrity of the data and the accuracy of the data analysis. PR, FRF and JS were responsible for the study concept and design. PR, DSP and AV contributed to the acquisition of data. MDMFA, MDLA and JMG performed the microglial morphology analysis. EB performed the object recognition test analysis. PR, AS, FJP, FRF and JS assisted with data analysis and interpretation of findings. PR, FRF and JS drafted of the manuscript. FRF and JS provided critical revision of the manuscript for important intellectual content, obtained funding and study supervision. All authors approved final version for publication.

ACKNOWLEDGEMENT

The authors thank to Evelin Vadas and Juan Antonio Fontalva Cruces for their technician support and assistance.

ABSTRACT

Changes in endogenous cannabinoid homeostasis are associated with ethanol-related neuroinflammation and memory decline. However, extensive research is required to unveil the role of cannabinoid activation on hippocampal microglial morphology, phenotyping and recruitment that may become notably altered by alcohol-related dementia. Here, we evaluated the pharmacological effects of the fatty-acid amide-hydrolase (FAAH) inhibitor URB597 (0.3 mg/kg) compared to oleoylethanolamide (OEA, 10 mg/kg), arachidonoylethanolamide (AEA, 10 mg/kg) and the selective CB1 and CB2 receptor agonists ACEA (3 mg/kg) and JWH133 (0.2 mg/kg), respectively, when they were administered for 5 days in a rat model of subchronic (2 weeks) ethanol exposure. Specifically, URB597 increased microglial (IBA-1+) cell population, and induces changes in morphometric features such as cell area and perimeter, roughness, fractal dimension and lacunarity associated with activated microglia in the hippocampus of ethanol-exposed rats. Regarding innate immune activity, URB597 specifically increased mRNA levels of toll-like receptor 4 (*TLR4*), glial fibrillary acidic protein (*Gfap*) and the chemokine stromal cell-derived factor 1 (*SDF-1α/CXCL12*), and elevated the cell population expressing the chemokine receptors CX3CR1, CCR2 and CCR4 in the ethanol-exposed rat hippocampus. Contrary to ethanol effect, URB597 reduced mRNA levels of *Iba-1*, *Tnfα*, *IL-6* and the monocyte chemoattractant protein 1 (*MCP-1/CCL2*), as well as the cell population expressing iNOS (a cytokine-inducible immune defense). Interestingly, URB597 effects on hippocampal immune system were accompanied by changes in short and long-term visual recognition memory. These results suggest that FAAH inhibition modulates hippocampal microglial recruitment and activation that can be associated with improved hippocampal-dependent memory despite ethanol exposure.

Key words: Alcohol; FAAH; hippocampus; memory, microglia

75 **1. INTRODUCTION**

76 Excessive alcohol consumption that results in cognitive and behavioral deficits may increase
77 the risk of dementia, especially among teenagers, given that heavy binge-drinking is
78 becoming a global burden of disease in young population (Guerri and Pascual, 2010;
79 Langballe et al., 2015). Substantial evidence in human and experimental animals has
80 demonstrated the vulnerability of the central nervous system to chronic ethanol exposure that
81 can cause irreversible changes in brain structure and functions such as synaptic plasticity and
82 neural connectivity (Pascual et al., 2018). Morphometric anomalies, such as smaller volume
83 of the prefrontal cortex, hippocampus and cerebellum (De Bellis et al., 2000, 2005), were
84 associated with axonal atrophy, cellular membrane breakdown and myelin loss in the brain of
85 heavy-drinking adolescents and adult alcoholics (Harper, 1998; Pfefferbaum et al., 2000). The
86 above structural changes in limbic system, such as the hippocampus with multipotent
87 progenitor cells that participate in learning and memory processes, have been correlated with
88 cognitive dysfunctions and neurophysiological abnormalities in heavy drinkers such as poorer
89 verbal declarative memory and alterations in attentional and visual working memories
90 (López-Caneda et al., 2013; Parada et al., 2011), affecting later social anxiety and drug self-
91 administration (van Praag et al., 2002; Spear, 2016). Neuropathological consequences induced
92 by alcohol drinking concomitantly occur with modifications in the innate immune system,
93 which markedly influence the refinement of dynamic processes during maturation stages that
94 finally impact on the adult brain functions (Montesinos et al., 2016).

95 New insights suggest alterations in the neuroimmune signaling in alcohol-induced brain
96 injury and long-lasting cognitive and memory consequences (Crews et al., 2015; Crews and
97 Vetreno, 2016). Neuroimmune cells, such as microglia and astrocytes, are important players
98 for neurocircuitry refinement and selective removal of unwanted synapses (pruning) during
99 adolescence (Schafer et al., 2015; Chung et al., 2015), as well as maintenance of normal

100 myelinogenesis in adulthood (Hagemeyer et al., 2017). Alcohol intake activates innate
101 immune response through toll-like receptor 4 (TLR4) in microglial cells, astrocytes and
102 macrophages by increasing the production of pro-inflammatory factors such as cytokines
103 (TNFα, IL-1β), chemokines (MCP-1, MIP-1α, eotaxin-1), reactive nitrogen and oxygen
104 species (Broadwater et al., 2014; García-Marchena et al., 2017; Pascual et al., 2018). In this
105 sense, HMGB1-TLR4 tolerance or sensitization and NF-κB target genes in monocytes and
106 macrophages becomes a pivotal role in ethanol-induced inflammatory cytokine production
107 and cognitive dysfunctions that depends on acute or repeated ethanol exposure (Montesinos et
108 al., 2015; Antón et al., 2017), for instance, becoming less or more responsive to
109 lipopolysaccharide stimulation (Afshar et al., 2015; Szabo and Saha, 2015).
110 Recent evidences indicate the importance of the endogenous cannabinoid and *N*-
111 acylethanolamine (NAE)-based signaling system (ECS) in many actions of alcohol on the
112 brain such as addiction, behavior, inflammation and neurogenesis (Serrano et al., 2012;
113 Rivera et al., 2015b; Bilbao et al., 2016; García-Marchena et al., 2016; Sánchez-Marín et al.,
114 2017). Considering this issue, a great deal of emphasis has been placed on evaluating the
115 effects of compounds targeting ECS (e.g. drugs modulating endocannabinoid tone) on the
116 adaptive and innate branches of the immune system (Sánchez and García-Merino, 2012;
117 Antón et al., 2017; Fernández-Ruiz et al., 2017). Endocannabinoids (eCBs) are lipid-derived
118 molecules that targeting to G protein-coupled cannabinoid type-1 and type-2 receptors (CB1
119 and CB2) may preserve glial cell subpopulations against numerous insults that disturb cell
120 homeostasis and integrity including excitotoxicity, mitochondrial dysfunction, proteostasis
121 and oxidative stress (Fernández-Ruiz et al., 2017). While how CB1 receptors regulate
122 microglia functions remains controversial, CB2 receptor up-regulation in conditions where
123 neuroinflammatory changes (e.g. Alzheimer's disease, multiple sclerosis) occurs as part of a
124 microglia activation process (Stella, 2009).

It is known that microglial function and morphology are closely related (Fernández-Arjona et al., 2017), but no studies have addressed this issue regarding the impact of eCB/NAE tone changes in ethanol-induced neuroinflammation and memory decline. We investigate the pharmacological effects of the repeated administration (5 days) of the NAEs hydrolyzing enzyme FAAH inhibitor URB597 (0.3 mg/kg), compared to OEA (10 mg/kg), AEA (10 mg/kg), ACEA (3 mg/kg) and JWH133 (0.2 mg/kg), in a rat model of subchronic (2 weeks) ethanol exposure. Microglia phenotyping (IBA-1, iNOS), morphometric parameters (*fractal dimension*, *lacunarity*, *roughness*, *cell area*, *cell perimeter*, *density*, among others), glial recruitment (chemokine receptors CX3CR1, CCR2, CCR4, CXCR4) and mRNA levels of cytokines related to innate immune TLR4 signaling (TNFα, IL-1β, IL-6) and chemotactic cytokines (fractalkine/CX3CL1, MCP-1/CCL2, SDF-1α/CXCL12, eotaxin-1/CCL11) were analyzed in the hippocampus of ethanol-exposed rats. Regarding behavior associated with hippocampal functioning, short and long-term visual recognition memory were also assessed.

2. MATERIALS AND METHODS

2.1. Ethics Statement

The protocols for animal care and use were approved by the Ethics and Research Committee at the Hospital Universitario Regional de Málaga and Universidad de Málaga. All experimental animal procedures were carried out in strict accordance with the European Communities directive 86⁄609⁄ECC (24 November 1986) and Spanish legislation (BOE 252⁄34367-91, 2005) regulating animal research. All efforts were made to minimize animal suffering and to reduce the number of animals used.

2.2. Animals

149 Male Wistar rats (approximately 250 g, 10–12 weeks old; Charles Rivers, Barcelona, Spain)
150 were housed individually in cages maintained in standard conditions (Centro de
151 Experimentación Animal, Universidad de Málaga) at 20 ± 2 ºC room temperature, 40 ± 5%
152 relative humidity and a 12-h light/dark cycle with dawn/dusk effect. Water and standard
153 rodent chow (Prolab RMH 2500, 2.9 kcal/g) were available *ad libitum*, unless otherwise
154 indicated for specific experimental procedures.

155

156 **2.3. Alcoholic diet habituation**

157 Seventy-two animals were daily weighed, handled for 10 minutes and habituated to injection
158 procedures (holding and pseudo-injection) during one week before the experimentation in
159 order to minimize stress effects. To habituate the animals to feeding procedures, rats were
160 first food-deprived to 95% of their free-feeding weight and then they were allowed *ad libitum*
161 access to a complete and balanced chocolate-flavored liquid food (0.97 kcal/mL; Glucerna
162 SR, Abbott Laboratories, Madrid, Spain) until a stable rate of feeding was reached (~50
163 mL/day, up to 2-3 days). Then, the rats were divided into two groups (*n*=36) and fed with the
164 chocolate-flavored liquid diet supplemented with 11% (*v/v*) ethanol 96º (alcoholic liquid diet)
165 or 14.7% (*w/v*) sucrose (sucrose liquid diet) (Serrano et al., 2012). Both alcoholic and sucrose
166 liquid diets were formulated to contain the same calories (1.4 kcal/mL). Thus, the same
167 volume of ethanol liquid diet consumed *ad libitum* was given the next day to the rats fed with
168 the sucrose liquid diet. The rats were maintained under a controlled-isocaloric per feeding
169 period until a stable rate of alcoholic feeding was reached (~30 mL/day, up to one week). In
170 any case, standard rodent chow was not given, but water was available *ad libitum*, during the
171 experimentation (see Rivera et al., 2015b for further details).

172

173 **2.4. Drug administration**

174 After alcoholic diet habituation, rats were fed *ad libitum* with both liquid diets (ethanol or
175 sucrose) and treated with the FAAH inhibitor URB597 (cyclohexyl carbamic acid 3'-
176 carbamoyl-biphenyl-3-yl ester; cat. no. 10046, Cayman Chemical, Ann Arbor, MI, USA), the
177 endogenous PPARα and GPR55 receptor agonist OEA (oleoylethanolamide; cat. no. 1484,
178 Tocris, Abingdon, UK), the endogenous cannabinoid and TRPV1 receptor agonist AEA
179 (arachidonoylethanolamide; cat. no. 1339, Tocris), the potent and highly selective CB1
180 receptor agonist ACEA (arachidonyl-2'-chloroethylamide; cat. no. 1319, Tocris), and the
181 potent and selective CB2 receptor agonist JWH133 (cat. no. 1343, Tocris). Drugs were
182 dissolved in a vehicle containing 33% (*v*/*v*) DMSO in sterile 0.9% NaCl solution, just before
183 each experiment, and were intraperitoneally (i.p.) injected in a final volume of 1 mL/kg of
184 body weight. The optimal dose at which treatment would be more effective in neuroprotection
185 was selected as described previously (Rivera et al., 2015a, 2015b). Thus, URB597, OEA,
186 AEA, ACEA and JWH133 were repeatedly administrated at respective doses of 0.3, 10, 10, 3
187 and 0.2 mg/kg body weight for 5 consecutive days at intervals of 24 hours (08:00 a.m.). The
188 animals were sacrificed 2 hours after the last injection of the drugs. Finally, we obtained
189 twelve experimental groups depending on the diet and treatment.

190

191 **2.5. Object recognition test**

192 The object recognition (OR) test was conducted to assess recognition memory during the
193 week of treatment (Ennaceur and Delacour, 1988). All testing was conducted in a 38 x 40 cm
194 opaque plastic rectangular arena with 54 cm high walls. One day before testing, animals
195 received a session in the experimental room for acclimatization. During the test, rats were
196 individually set into the arena where two identical objects were placed. Animals were allowed
197 to explore the apparatus and the objects for 10 min (sample trial). Two hours (short-term) and
198 twenty-four (long-term) hours later, the rats were then returned twice more to the arena and

199 were presented with one familiar object and one novel object. The animals were allowed to
200 explore the apparatus and objects for 10 min (retention trial; Pezze et al., 2015). The
201 apparatus was evenly illuminated at approximately 70 lux and the device and the objects were
202 thoroughly clean between trials. All possible location or object combinations were employed
203 to prevent bias due to a preference for a particular object or specific location by using a
204 counterbalanced procedure within treatment groups. Animals were considered to be exploring
205 an object when their snout was directed towards it at a distance of 2 cm or less. The time
206 spent (duration), distance and frequency exploring the objects by rats were scored using a
207 video monitor. Discrimination index (d1) was calculated using the following formula: d1 = N
208 / (N + F), where N is the amount of time that rats expend exploring the novel object and F is
209 the amount of time that rats explore the familiar object. The same formula was applied for
210 distance (space surrounding the object) and frequency (times of snout touching on object) of
211 exploration.
212
213 **2.6. Sample collection**
214 Previous to sacrifice, all animals were i.p. anaesthetized (sodium pentobarbital, 50 mg/kg
215 body weight) in a room separate from the other experimental animals. The animals were
216 sacrificed by decapitation and their brains were collected, quick frozen and stored at −80 °C.
217 These brains were then disected on dry ice to obtain sections of 1 mm thick by using razor
218 blades and a rat brain slicer matrix. The dorsal hippocampus was precisely removed from -
219 2.16 to -4.20 mm of Bregma levels (Paxinos and Watson, 2007) with fine surgical
220 instruments. Hippocampal samples were weighed and stored at −80 °C until they were used
221 for real time quantitative polymerase chain reaction (RT-qPCR) analysis. A replicated batch
222 of rats were transcardially perfused with 4% formaldehyde in 0.1 M phosphate buffer (PB),
223 and the brains were dissected and kept in the same fixative solution overnight at 4 ºC. The

224 brains were cryoprotected and cut into 30-µm-thick coronal sections using a sliding
225 microtome (Leica VT1000S). Sections were divided in eight parallel series until use for
226 immunostaining.
227

228 **2.7. RNA isolation and RT-qPCR analysis**

229 We performed RT-qPCR (TaqMan, Applied Biosystem, Carlbad, CA, USA) as described
230 previously (Rivera et al., 2015a) using specific sets of primer probes (see **Table S1**). Briefly,
231 hippocampal samples were homogenized on ice and RNA was extracted following
232 Trizol® method according to the manufacture's instruction (Gibco BRL Life Technologies,
233 Baltimore, MD, USA). RNA samples were isolated with RNAeasy minelute cleanup-kit
234 including digestion with DNase I column (Qiagen, Hilden, Germany). After reverse transcript
235 reaction from 1 µg of mRNA, quantitative real-time reverse transcription polymerase chain
236 reaction (qPCR) was performed in a CFX96TM Real-Time PCR Detection System (Bio-Rad,
237 Hercules, CA, USA) and the FAM dye label format for the TaqMan® Gene Expression
238 Assays (ThermoFisher). Melting curve analysis was performed to ensure that only a single
239 product was amplified. Ct values were normalized in relation to *Gapdh* mRNA levels.
240

241 **2.8. Immunohistochemistry**

242 Free-floating coronal sections from -2.16 to -4.20 mm of Bregma levels were selected (Rivera
243 et al., 2015a). Sections were incubated overnight at 4 ºC in the following diluted primary
244 antibodies: polyclonal rabbit anti-IBA-1 (1:1000, Wako, cat. no. 019-19741), monoclonal
245 mouse anti-iNOS (10 µg/mL, R&D Systems, cat. no. MAB9502), monoclonal mouse anti-
246 GFAP (1:500, Sigma-Aldrich, cat. no. G3893), polyclonal rabbit anti-CX3CR1 (1:500,
247 Abcam, cat. no. ab8021), polyclonal rabbit anti-CCR2 (1:300, Novus Biologicals, cat. no.
248 NBP1-78169), polyclonal rabbit anti-CCR4 (1:300, Novus Biologicals, cat. no. NB100-

249 56336) and monoclonal rabbit anti-CXCR4 (1:300, Abcam, cat. no. ab124824). The following
250 day the sections were washed and incubated in biotinylated donkey anti-rabbit IgG (1:500,
251 GE Healthcare, cat. no. RPN1004) at room temperature for 1.5 h. Then, sections were
252 incubated in ExtrAvidin peroxidase (Sigma-Aldrich) diluted 1:2000 in darkness at room
253 temperature for 1 h. Finally, immunolabeling was revealed with 0.05% diaminobenzidine
254 (DAB, Sigma-Aldrich), 0.05% nickel ammonium sulfate (Ni) and 0.03% H_2O_2 in PB-saline
255 for 10 min.

256

257 **2.9. Stereological cell quantification**

258 The average density of immunoreactive cells per animal was manually quantified using
259 stereological methods. Estimations of the number of cells per sections (30 µm deep) and area
260 (mm^2) in both hemispheres were calculated according to the following formula: $N_a = \Sigma(Q\text{-})/$
261 $\Sigma(a_{str})$, where ΣQ- is the total number of positive (+) cells counted per animal, and a_{str} is the
262 area of the structure analyzed. Each structure analyzed consisted of approximately 8 coronal
263 sections (from -2.16 to -4.20 mm Bregma levels), which resulted in one of every eight
264 equidistant sections (one representative section for each 240 µm) according to the rostro-
265 caudal extent. IBA-1+, iNOS+, GFAP+, CX3CR1+, CCR2+, CCR4+ and CXCR4+ cell
266 counts were performed in the dentate gyrus (DG) and CA3 and CA1 hippocampal areas.
267 Representative counting frames were evaluated using a standard optical microscope with the
268 40x objective (Nikon Instruments Europe B.V., Amstelveen, The Netherlands) coupled to the
269 NIS-Elements Imaging Software 3.00 (Nikon). Quantification was expressed as the average
270 number of positive cells per area (mm^2) for each experimental group.

271

272 **2.10. Morphometric analysis**

273 For image acquisition, digital color images of DG sections immunolabeled with IBA-1
274 antibody and DAB-Ni were obtained using an Olympus VS120 microscope. The UPLSAPO
275 60xO oil immersion objective was used to capture high resolution images (pixel size = 115
276 mm^2) of the selected areas. A multi-plane virtual-Z mode allowed to capture 20 images (1 µm
277 thick) in 20 µm depth of the section, which were later combined to obtain a single high
278 quality image including detailed magnification of ramified processes of the cells. Each
279 scanned image was a TIFF file of 96 ppi, and contained at least 30 cells.

280 For image processing, individual microglial cells were selected and cropped from the
281 captured images according to the following criteria (**Figure S1A**): (i) random selection
282 throughout the molecular layer of the DG; (ii) no overlapping with neighboring cells, and (iii)
283 complete nucleus and branches (at least apparently). Selection was done blinded to diet or
284 treatment. Approximately 50 cells selected from 6 animals were analyzed for each
285 experimental condition. Each single cell image was processed in a systematic way using *FIJI*
286 free software (freely downloadable from https://imagej.net/Fiji) to finally obtain a "filled
287 image" and its counterpart "outlined shape" (**Figure S1B**) as previously described
288 (Fernández-Arjona et al., 2017).

289 These filled and outlined cell images were subsequently used for morphometric analysis.
290 Morphological features of microglial cells were quantified with the free software *FracLac* for
291 *ImageJ* (Karperien, A., FracLac for ImageJ; available at the ImageJ website, NIH). The
292 following 15 parameters were measured (**Figure S1C**) as previously described by Fernández-
293 Arjona et al (2017): *fractal dimension* (*D*), *lacunarity* (Λ), *cell area* (CA, μm^2), *convex hull*
294 *area* (CHA, μm^2), *density* (CA/CHA), *cell perimeter* (CP, µm), *convex hull perimeter* (CHP,
295 µm), *roughness* (CP/CHP), *convex hull span ratio*, *cell circularity* [CC = $(4\pi \cdot CA)/(CP)^2$],
296 *maximum mass center radius*, *diameter of the bounding circle* (µm), *maximum span across*

297 *the convex hull* (µm), *the ratio maximum/minimum convex hull radii* and *the mean radius*
298 (µm).
299

300 **2.11. Statistical analysis**

301 Comparisons of data were carried out using SPSS Statistics software and GraphPad Prism
302 version 5.04 software (GraphPad Software, San Diego, CA, USA). Data are expressed as
303 mean ± SEM for at least six determinations per experimental group (see figure legends in
304 each case). The Kolmogorov-Smirnov normality test, along with the Levene homoscedasticity
305 test, were used to verify Gaussian distribution. Statistical analyses were performed using a
306 two-way analysis of variance (ANOVA) with two factors being diet (sucrose and ethanol) and
307 treatment (vehicle, URB597, OEA, AEA, ACEA and/or JWH133). The Kruskal-Wallis test
308 was performed for the non-parametric data. In the pairwise comparison Tuckey's test was
309 used when possible. A *p*-value less than 0.05 was considered statistically significant.
310

311 **3. RESULTS**

312 **3.1. URB597 and AEA increased the number of microglial IBA-1+ cells in the**
313 **hippocampus**

314 Rats exposed to ethanol (10%) for 2 weeks were treated with OEA (10 mg/kg), JWH133 (0.2
315 mg/kg), ACEA (3 mg/kg), AEA (10 mg/kg) and URB597 (0.3 mg/kg) for 5 days. Two-way
316 ANOVA (ethanol and treatment as factors) indicated treatment effects on the number of cells
317 expressing IBA-1 in the DG, CA3, CA1 and the whole hippocampus ($F_{5,104} > 27.3$, $p <$
318 0.0001). An ethanol effect on the number of IBA-1+ cell was only observed in CA3
319 hippocampal area ($F_{1,104} = 9.77$, $p = 0.0023$), but not in the remaining hippocampal regions
320 analyzed. Interaction between factors was found in the CA3 and CA1 hippocampal areas and

321 the whole hippocampus ($F_{5,104} > 2.71$, $p < 0.023$), suggesting that treatment effect on IBA-1+
322 cell population is ethanol dependent.
323 Regarding *post-hoc* analysis, AEA and URB597 increased the number of IBA-1+ cells in the
324 whole hippocampus, including DG, and CA3 and CA1 hippocampal areas, of sucrose-
325 exposed rats, excepting CA3 of AEA-treated rats (*/**/****p*<0.05/0.01/0.001), and ethanol-
326 exposed rats ($^{###}p$<0.001) compared to that of the respective sucrose and ethanol-vehicle rats
327 (**Fig. 1A-D**). In ethanol-exposed rats, OEA and JWH133 specifically increased the IBA-1+
328 cell population in CA3 area and whole hippocampus ($^{#}p$<0.05; **Fig. 1C,D**), as well as
329 JWH133 in the DG ($^{#}p$<0.05; **Fig. 1A**), compared to ethanol-vehicle rats. In contrast, OEA
330 and JWH133 specifically decreased the IBA-1+ cell population in CA3 area of sucrose-
331 exposed rats compared to sucrose-vehicle rats (**p*<0.05; **Fig. 1B**). Representative images of
332 hippocampus are shown in **Figure 1E-P**.
333
334 **3.2. URB597 induces morphometric changes in microglial IBA-1+ cells of dentate gyrus**
335 We also analyzed the effects of OEA, JWH133, ACEA, AEA and URB597 on morphologic
336 parameters of microglial cells expressing IBA-1 in the dentate gyrus (DG) of ethanol-exposed
337 rats compared to those of sucrose-exposed ones. Two-way ANOVA indicated treatment
338 effects on main morphometric parameters such as *cell area* (CA), *cell perimeter* (CP), *density*,
339 *roughness*, *fractal dimension* and *lacunarity* ($F_{5,605} > 10.58$, $p < 0.0001$), as well as the related
340 parameters CHA, CHP, maximum span across the convex hull, *diameter of the bounding*
341 *circle*, and the *ratio maximum/minimum convex hull radii* ($F_{5,605} > 2.28$, $p < 0.044$).
342 Prominent effects of ethanol on CP, CHA, CHP, *density*, *roughness*, *fractal dimension*,
343 *maximum span across the convex hull*, *convex hull span ratio*, *diameter of the bounding*
344 *circle*, *the maximum mass center radius* and *the mean radius* ($F_{1,605} > 12.33$, $p < 0.0005$), as
345 well as CA and *lacunarity* ($F_{1,605} > 4.51$, $p < 0.034$), were also found. Interaction between

346 factors was observed in CA, CHA, CP, *roughness*, *fractal dimension*, *maximum span across*
347 *the convex hull* and *diameter of the bounding circle* ($F_{5,605} > 2.23$, $p < 0.049$), suggesting that
348 treatment effect on microglial morphology is ethanol dependent.
349 Regarding *post-hoc* analysis, ethanol specifically increased *roughness* of DG microglial cells
350 in vehicle-treated rats compared to that of sucrose-vehicle ones ($^{###}p<0.001$; **Fig. 2D**).
351 URB597, but not the remaining drugs, increased CA, CP, *density*, roughness and *fractal*
352 *dimension* of microglial cells in DG of both sucrose and ethanol-exposed rat groups
353 ($^{***}p<0.001$; **Fig. 2A-E**). AEA also increased CA and *density* of microglial cells in DG of
354 ethanol-exposed rats ($^{***}p<0.001$; **Fig. 2A,C**). In contrast, both AEA and URB597
355 specifically reduced *lacunarity* in microglial cells in DG of ethanol-exposed rats ($^{*}p<0.05$;
356 **Fig. 2F**). CA was increased in ethanol-exposed rats treated with AEA, as well as CP and
357 *roughnes*s in ethanol-exposed rats treated with JWH133 and AEA, when they were compared
358 to those of sucrose-exposed rats treated with the respective JWH133 and AEA ($^{###}p<0.001$;
359 **Fig. 2A,B,D**). In contrast, *fractal dimension* was reduced in ethanol-exposed rats treated with
360 ACEA and URB597 compared to that of sucrose-exposed rats with the same treatments
361 ($^{###}p<0.001$; **Fig. 2E**). No significant changes in the remaining morphometric parameters were
362 induced by OEA, JWH133, ACEA, AEA and URB597 in sucrose and ethanol-exposed rats
363 (**Fig. S2**).
364

365 **3.3. URB597 decreased the microglial iNOS+ cell subpopulation in the hippocampus**

366 We also evaluated the effects of OEA, JWH133, ACEA, AEA and URB597 on the number of
367 resident innate immune cells expressing iNOS (a cytokine-inducible immune defense) and
368 GFAP (astroglia) in the hippocampus of ethanol-exposed rats. Two-way ANOVA indicated
369 treatment effects on the number of iNOS+ cells in the DG, CA3, CA1 and the whole
370 hippocampus ($F_{5,104} > 5.69$, $p < 0.0002$). An ethanol effect on the number of iNOS+ cell was

371 only observed in DG and CA1 ($F_{1,104} > 4.93$, $p < 0.028$), but not in CA3 and the whole
372 hippocampus. Interaction between factors was found in the DG, CA3, CA1 and the whole
373 hippocampus ($F_{5,104} > 4.44$, $p < 0.001$), suggesting that treatment effect on iNOS+ cell
374 population is ethanol dependent.

375 Ethanol reduced the number of cells expressing iNOS in the DG, CA3, CA1 and the whole
376 hippocampus compared to that of sucrose-vehicle ones (*/***p*<0.05/0.01; **Fig. 3A-D**). All
377 treatments (OEA, JWH133, ACEA, AEA and URB597) reduced the number of iNOS+ cells
378 in the DG of sucrose-exposed rats compared to that of sucrose-vehicle rats
379 (*/****p*<0.05/0.001; **Fig. 3A**). AEA and URB597 also decrease the number of iNOS+ cells in
380 CA3, CA1 and the whole hippocampus in the same rats (*/**/****p*<0.05/0.01/0.001; **Fig. 3B-**
381 **D**). Moreover, OEA also reduced the iNOS+ cell population in CA3 area and the whole
382 hippocampus in sucrose-exposed rats (****p*<0.001; **Fig. 3B,D**). However, the number of
383 iNOS+ cells in JWH133-treated, sucrose-exposed rats was also lower in CA3 but higher in
384 CA1 compared to those of sucrose-vehicle rats (*/***p*<0.05/0.01; **Fig. 3B,C**). Regarding
385 ethanol-exposed rats, URB597 specifically reduced the iNOS+ cell population in DG and the
386 whole hippocampus ($^{\#/\#\#}p<0.05/0.01$; **Fig. 3A,D**), whereas AEA increased iNOS+ cell
387 population in CA1 hippocampal area compared to ethanol-vehicle rats ($^{\#}p<0.05$; **Fig. 3C**).
388 Representative images of DG are shown in **Figure 3E-P**.

389

390 **3.4. URB597 decreased the number of astroglial GFAP+ cells in the hippocampus**

391 Treatment effects on the number of GFAP+ cells (astrocytes) were found in the DG, CA3,
392 CA1 and the whole hippocampus ($F_{5,104} > 43.87$, $p < 0.0001$). Ethanol effect and interaction
393 were not observed.

394 While URB597 reduced the number of cells expressing GFAP in the DG, CA3, CA1 and the
395 whole hippocampus of both sucrose and ethanol-exposed rat groups, AEA increased it in all

396 hippocampal regions of both rat groups compared to the respective vehicle rats
397 (*/**/***p<0.05/0.01/0.001, $^{\#\#\#}$p<0.001; **Fig. 4A-D**). In sucrose-exposed rats, OEA, JWH and
398 ACEA also increased GFAP+ cell population in the DG and the whole hippocampus
399 (*/***p<0.05/0.001; **Fig. 4A,D**). In ethanol-exposed rats, JWH133 and ACEA increased the
400 number of GFAP+ cells in the DG, and only JWH133 in the whole hippocampus, compared
401 to vehicle ones ($^{\#\#/\#\#\#}$p<0.01/0.001; **Fig. 4A,D**). Representative images of hippocampus are
402 shown in **Figure 4E-P**.
403
404 **3.5. URB597 modulates hippocampal gene expression of cytokines and chemokines**
405 **related to innate immune TLR4 system**
406 We evaluated innate immune system related to TLR4 that regulates the gene expression of
407 cytokines (*Iba-1*, *Tnfα*, *IL-1β*, *IL-6*) and chemokines (*SDF-1α*, *MCP-1*, *eotaxin-1*,
408 *fractalkine*). Treatment effects on mRNA levels of *TLR4* ($F_{1,24} = 7.2$, $p = 0.013$), *Iba-1* ($F_{1,24}$
409 $= 30.06$, $p < 0.0001$), *Tnfα* ($F_{1,24} = 34.13$, $p < 0.0001$), *SDF-1α* ($F_{1,24} = 6.96$, $p = 0.014$) and
410 *MCP-1* ($F_{1,24} = 16.23$, $p = 0.0005$) were found in the hippocampus. We only detected ethanol
411 effects on mRNA levels of *Iba-1* ($F_{1,24} = 9.88$, $p = 0.004$) and *Tnfα* ($F_{1,24} = 4.90$, $p = 0.036$),
412 as well as interaction between factors in mRNA levels of *Iba-1* ($F_{1,24} = 9$, $p = 0.006$), *IL-6*
413 ($F_{1,24} = 6.84$, $p = 0.015$) and *MCP-1* ($F_{1,24} = 4.89$, $p = 0.03$). Later results suggest that
414 URB597 affects hippocampal *Iba-1*, *IL-6* and *MCP-1* gene expression levels in an ethanol-
415 dependent manner.
416 Specifically, mRNA levels of *Iba-1*, *Tnfα*, *IL-6* and *MCP-1* were increased in the
417 hippocampus of ethanol-exposed rats compared to those of sucrose-exposed rats
418 (*/****p*<0.05/0.001; **Fig. 5A,B**). In the hippocampus of ethanol-exposed rats, URB597
419 decreased mRNA levels of *Iba-1*, *Tnfα*, *IL-6* and *MCP-1*, and increased mRNA levels of
420 *TLR4*, *Gfap* and *SDF-1α* compared to those of vehicle-treated rats ($^{\#/\#\#/\#\#\#}$*p*<0.05/0.01/0.001;

421 **Fig. 5A,B**). *Tnfα* gene expression was also decreased in sucrose-exposed rats treated with
422 URB597 compared to vehicle ones (***p<0.001; **Fig. 5A**).
423
424 **3.6. URB597 increases the number of microglial cells expressing the chemokine**
425 **receptors CX3CR1, CCR2 and CCR4**
426 We found treatment effects on the number of cells expressing CX3CR1, CCR2 and CCR4 in
427 the whole hippocampus ($F_{1,20} > 23.70$, $p < 0.0001$), including DG, CA3 and/or CA1
428 hippocampal regions (DG: $F_{1,20} > 9.79$, $p < 0.006$; CA3: $F_{1,20} > 5.87$, $p < 0.02$; CA1: $F_{1,20} >$
429 14.10, $p < 0.002$). No treatment effects on the number of CA3 CCR4+ cells and hippocampal
430 CXCR4+ cells were found. We also observed ethanol effects on the number of CX3CR1+
431 cells in the DG, CA1 and the whole hippocampus ($F_{1,20} > 11.41$, $p < 0.004$), the number of
432 CCR2+ cells in the whole hippocampus ($F_{1,20} = 5.20$, $p = 0.033$), the number of CCR4+ cells
433 in CA3 ($F_{1,20} = 7.40$, $p = 0.013$), and the number of CXCR4+ cells in CA1 ($F_{1,20} = 7.69$, $p =$
434 0.011). Interaction between factors was found in the number of CX3CR1+ cells in the DG
435 ($F_{1,20} = 5.98$, $p = 0.023$) and the whole hippocampus ($F_{1,20} = 8.36$, $p = 0.009$), and in the
436 number of CCR2+ cells in the whole hippocampus ($F_{1,20} = 7.96$, $p = 0.01$). Later results
437 suggest that URB597 differentially affected the hippocampal cell population expressing
438 CX3CR1 and CCR2 in an ethanol-dependent manner. No interaction was observed in CCR4+
439 and CXCR4+ cell populations.
440 Regarding *post-hoc* analysis, the number of CX3CR1+ cells were reduced in the DG, CA3
441 and the whole hippocampus of ethanol-exposed rats compared to those of sucrose ones
442 (**/***p<0.01/0.001; **Fig. 6A**). In contrast, the number of CCR4+ cells were specifically
443 increased in CA3 of the same ethanol-exposed animals (**p<0.01; **Fig. 6C**). In sucrose-
444 exposed rats, URB597 increased the CX3CR1+ cells population in CA1, the CCR2+ cells
445 population in the DG, CA3, CA1 and the whole hippocampus (**Fig. 6A**), and the CCR4+ cell

446 population in CA1 (**Fig. 6B**) and the whole hippocampus (**Fig. 6C**) compared to vehicle ones
447 (*/**/***p<0.05/0.01/0.001). In contrast, the number of CXCR4+ cells was specifically
448 decreased in the DG of sucrose-exposed rats treated with URB597 (*p<0.05; **Fig. 6D**). In
449 ethanol-exposed rats, URB597 increased the number of CX3CR1+ cells in the DG, CA3, CA1
450 and the whole hippocampus (**Fig. 6A**), the number of CCR2+ cells in CA1 and the whole
451 hippocampus (**Fig. 6B**), and the number of CCR4+ cells in the DG, CA1 and the whole
452 hippocampus (**Fig. 6C**) of ethanol-exposed rats compared to those of vehicle ones
453 ($^{\#\#/\#\#\#}p<0.01/0.001$). Representative images of DG are shown in **Figure 6E-H**.
454

455 **3.7. URB5097 improves short-term and long-term memory in ethanol-exposed rats**

456 We evaluated whether changes in microglial population, morphology and phenotyping related
457 to innate immune system in the hippocampus of ethanol-exposed rats are associated with
458 hippocampal behavioral functioning such as recognition memory. To this aim, we used a
459 discrimination index [N/(N+F)] in parameters (distance, duration, frequency,
460 duration/frequency) obtained from short-term and long-term object recognition (OR) tests.
461 We found an ethanol effect on frequency in short-term OR test ($F_{1,20} = 12.31$, $p = 0.002$), and
462 on distance ($F_{1,20} = 4.25$, $p = 0.05$), duration ($F_{1,20} = 50.07$, $p < 0.0001$) and
463 duration/frequency ratio ($F_{1,20} = 4.43$, $p = 0.048$) in long-term OR test. Interactions between
464 factors (ethanol and URB597) in duration/frequency ratio were observed in short-term ($F_{1,20}$ =
465 4.62, $p = 0.043$) and long-term ($F_{1,20} = 8.22$, $p = 0.009$) recognition memory.

466 Rats exposed to ethanol showed an increased frequency in short-term OR test and an
467 increased duration in long-term OR test compared to sucrose ones (***p<0.001; **Fig. 7A,B**).
468 Ethanol specifically reduced duration/frequency ratio in short-term, but not long-term, OR
469 test (*p<0.05; **Fig. 7A,B**). URB597 increased duration/frequency ratio in both short-term and
470 long-term OR tests in ethanol-exposed rats compared to vehicle ones ($^{\#}p<0.05$; **Fig. 7A,B**).

471 Additionally, distance and duration in short-term OR test as well as duration and
472 duration/frequency ratio in long-term OR test were elevated in URB597-treated ethanol-
473 exposed rats compared to URB597-treated sucrose-exposed rats (*/***$p<0.05/0.001$). In
474 contrast, distance in long-term OR test was decreased in the same animals (*$p<0.05$; **Fig. 7B**).
475

476 **4. DISCUSSION**

477 In the present study, we show that, among other cannabinoid activators with less or more
478 selective binding to CB1 or CB2 receptors (AEA, ACEA, JWH133) as well as other *N*-
479 acylethanolamides such as OEA binding to PPARα, the FAAH inhibitor URB597 induced the
480 most consistent changes in morphology (fractal analysis), phenotyping related to innate
481 immune TLR4 system (TLR4, TNFα, IL-6) and glial recruitment through chemokines (SDF-
482 1α/CXCL12, MCP-1/CCL2) and chemokine receptors (CX3CR1, CCR2 and CCR4), in
483 hippocampal microglia of rats exposed to ethanol. These effects on microglial activity are
484 likely associated with an improvement of visual recognition memory despite ethanol
485 exposure. To our knowledge, this is the first study that evaluate the influence of cannabinoids
486 and ethanol on microglial phenotyping, morphology and hippocampal-dependent memory.
487

488 **4.1. Ethanol effects on neuroinflammatory signaling and microglial morphology**

489 Seminal studies demonstrated that alcohol induced changes in glial activation and immune
490 signaling, affecting brain structure and function (Crews et al., 2006). Repeated ethanol
491 drinking increases the expression of different components of neuroimmune system such as
492 innate immune receptors (TLR3, TLR4) and the production of NF-κB-related pro-
493 inflammatory molecules including cytokines (i.e. TNFα, IL-1β, IL-6), chemokines (MCP-1,
494 eotaxin-1), and nitric oxide resulting in neuroinflammation and oxidative stress (Stellwagen
495 and Malenka, 2006; Qin and Crews, 2012; Antón et al., 2016; García-Marchena et al., 2017;

496 Sanchez-Marín et al., 2017; Pascual et al., 2018). In the present study, mRNA levels of *Iba-1*
497 as well as the cytokines *Tnfα* and *IL-6* were increased in the hippocampus of rats exposed to
498 ethanol for 2 weeks. Previous studies have not observed changes in *Tnfa*, *IL-6* and *Tlr4*
499 mRNA levels, but described increases in *Iba-1* mRNA levels and decreases in *Gfap* mRNA
500 levels in adolescent and adult rodent hippocampus exposed to several binge drinking episodes
501 (Marshall et al., 2013; Kane et al., 2014; Sánchez-Marín et al., 2017). Moreover, recent
502 studies (Cruz et al., 2017; Pradier et al., 2018) suggest that long-term ethanol exposure (20%
503 or 11 g/kg) for up to 12 months promotes cytokine production (IL-1β, IL-15, TNFα) and
504 induces a partial activation and increased density of microglia (CD11b, IL-1β).
505 Microglia, brain immune cells which contain ramified and dynamically moving processes,
506 constantly surveil the brain parenchyma to detect dysfunction (Nimmerjahn et al., 2005).
507 Microglia-related immunoinflammatory mechanisms include traveling to the sites of injury,
508 following chemoattractive signals (chemokines), where they can recruit or activate other cells
509 including processes such as proliferation, apoptosis and phagocytosis that contribute to neural
510 repair and reorganization (He and Crews, 2008). Studies using animal models of alcoholism
511 (Kane et al., 2014; Anton et al., 2017) and human alcoholics (He and Crews, 2008) indicated
512 increased concentrations of the chemoattractant protein MCP-1 in the brain including
513 hippocampus. We observed that ethanol exposure for 2 weeks increased *MCP-1/CCL2*
514 mRNA levels, but not other chemokines such as *SDF-1α/CXCL12*, *eotaxin-1/CCL11* and
515 *fractalkine/CX3CL1* in the hippocampus of our rat model. Additionally, ethanol reduced the
516 number of cells expressing iNOS (a cytokine-inducible immune defense) and the number of
517 cells expressing the chemokine receptor CX3CR1 (fractalkine receptor) in the hippocampus.
518 No overall changes were found in hippocampal populations of glial cells expressing IBA-1
519 (microglia) and GFAP (astroglia), as well as in the number of hippocampal cells expressing
520 CCR2 (MCP-1 receptor), CCR4 (CCL17/CCL22 receptor) and CXCR4 (SCD-1α receptor).

521 Concerning the role of immune system in subjects with alcohol use disorders (AUD), alcohol
522 consumption has been shown to affect cytokines and chemokines (Cui et al., 2011; García-
523 Marchena et al., 2017). A recent study in patients with AUD revealed a link of the eosinophil
524 chemotactic protein eotaxin-1/CCL11 with psychiatric comorbidity and a strong sex effect
525 (García-Marchena et al., 2017). These authors also described that rats exposed to repeated and
526 acute ethanol (3 g/kg, gavage) had changes in circulating concentrations of SDF-1α/CXCL12,
527 fractalkine/CX3CL1 and eotaxin-1/CCL11 (García-Marchena et al., 2017)
528 It is well established that microglial function and form by a variety and complex
529 morphologies (ramified/intermediate/activated) are inextricably linked (Karperien et al., 2013;
530 Fernández-Arjona et al., 2017). When abnormality in the brain function is present, microglia
531 result in a changed morphology to be active in an inflammatory response (Morrison et al.,
532 2017). Thus, the objective quantification of microglial morphology (fractal analysis) provides
533 an essential tool to discriminate the resting, quiescent or activated (reactive) form of microglia
534 (Soltys et al., 2005; Eggen et al., 2013). In the present study, ethanol effect on microglial
535 morphology was consistent in most morphometric parameters analyzed, suggesting a decrease
536 in *density*, *fractal dimension* and *lacunarity*. These results indicate that the morphologically
537 and functionally dynamic microglia, when they are exposed to ethanol, mostly remain in a
538 low ramified form with decreasing complexity of branching patterns that implies
539 homogeneity in shape. These features likely agree with morphological categories of de-
540 ramifying and/or activated microglia (Karperien et al., 2013; Fernández-Arjona et al., 2017).
541
542 **4.2. URB597 effects on neuroinflammatory signaling and microglial morphology**
543 The neuroprotective properties of compound targeting the endocannabinoid system include a
544 modulatory effect on innate immune system. Several studies have supported the ability of
545 cannabinoid activation (e.g. delta-9-tetrahydrocannabinol) to decrease inflammation with

546 recent evidence indicating that neuroimmune changes, including microglial activation, were
547 more profound in mice lacking CB2 receptor (Ehrhart et al., 2005; Palazuelos et al., 2008).
548 Selective CB2 receptor activation prevents deficits in microglial activation and cognitive
549 impairment, including the undesired psychoactive effects of neuronal CB1 receptor
550 stimulation (Rom and Persidsky, 2013). URB597, which by decreasing *N*-acylethanolamine
551 hydrolysis lead to increased endocannabinoid tone including AEA and OEA, was described to
552 attenuate age-related microglial activation such as the microglial markers MHCII, CD11b,
553 CD68 and CD40 associated with decreases in mRNA levels of the proinflammatory cytokines
554 *Tnfα* and *IL-1β* (Murphy et al., 2012), and reduced the number of microglial cells expressing
555 IBA-1 (Rivera et al., 2015a) in the hippocampus of naïve rats. Consistently, a number of *in*
556 *vivo* and *in vitro* studies have demonstrated that endocannabinoids and/or cannabinoid-like
557 synthetic molecules (e.g. WIN-55,212-2) reduced microglial activation in brain of animals
558 which received neurotoxic stimuli such as amyloid-β, interferon-γ or lipopolysaccharide
559 (Ehrhart et al., 2005; Roche et al., 2008; Ramirez et al., 2013). Similarly, our study indicates
560 that URB597 attenuated the ethanol-induced increase in mRNA levels of the proinflammatory
561 cytokines and chemokines *Iba-1*, *Tnfα*, *IL-6* and *MCP-1*. Decreased neuroinflammation
562 induced by URB597 can be likely associated with decreases in the number of GFAP+ cells
563 (astrocytes) and glial cells expressing the immune response marker iNOS. Astrocytes also
564 function as resident immune cells in the brain and can induce an inflammatory response by
565 producing pro-inflammatory molecules (cytokine and chemokines) in a region-specific
566 manner (Kane et al., 2014). For instance, MCP-1 is a chemokine highly expressed in
567 astrocytes that is able to alter addiction to alcohol (Blednov et al., 2005). Specifically, ethanol
568 administration (6 g/kg) via gavage for 10 days increased mRNA levels of *MCP-1* in the
569 hippocampus and resulted in increased GFAP immunostaining (Kane et al., 2014).

570 In the hippocampus of ethanol-exposed rats, URB597 induced a specific increase in the
571 mRNA levels of *TLR4*, an inflammatory signaling system that plays a fundamental role in
572 pathogen recognition and activation of innate immunity. Recently, special emphasis is given
573 to the actions of ethanol in the inflammatory TLR4/NF-κB signaling response in glial cells
574 triggering cytokines and chemokines (Pascual et al., 2017). In this sense, OEA was described
575 to prevent neuroimmune HMGB1/TLR4/NF-κB signaling in the rat frontal cortex induced by
576 ethanol binge administration (Antón et al., 2016).
577 Among a variety of available drugs affecting cannabinoid activity and *N*-acylethanolamine
578 tone (i.e. AEA, ACEA, JWH133, OEA, URB597), both AEA and URB597 increased the
579 number of microglial cells expressing IBA-1 in the hippocampus under an alcoholic context,
580 suggesting a role of cannabinoid receptors in microglial recruitment and activation following
581 specific neurotoxic stimuli. These results agree with enhanced microglial density in the
582 hippocampus of *faah*$^{-/-}$ mice (Ativie et al., 2015). In agreement with this observation,
583 URB597 increased mRNA levels of the chemokine *SDF-1α*, but not changes were found in
584 *eotaxin-1* and *fractalkine* in the hippocampus of ethanol-exposed rats. Additionally, URB597
585 increased the hippocampal cell population expressing the chemokine receptors CX3CR1,
586 CCR2 and CCR4. Several studies indicated that accumulation of microglia is associated with
587 increased mRNA expression of *Cnr2* (CB2 receptor), *CX3CR1* and *CCR2* under specific
588 neurodegenerative conditions, effects on microglia that were inhibited by cannabinoid
589 activation (Fernández-López et al., 2012). However, under an alcoholic context, *Cnr2* mRNA
590 levels were specifically decreased in the rat hippocampus (Sánchez-Marín et al., 2017),
591 suggesting a different modulatory role of the endocannabinoid system in ethanol-related
592 neuroinflammation. In this sense, special attention should be given to CX3CR1 role in
593 neuroinflammation as rising hypothesis suggests that CB2 receptor activation (i.e. JWH133)

594 accelerates CX3CR1+ microglia secreting neurotrophic factors and restores damaged
595 neuronal circuit (Tang et al., 2017).
596 URB597 also promotes morphologic changes in microglia. Changes in relevant morphometric
597 parameters suggest that URB597 likely modulate ethanol-related microglial activation by
598 enhancing *cell area*, *cell perimeter*, *roughness* and *lacunarity* (less polarization), and
599 reverting ethanol-induced decreased *density* and *fractal dimension* (higher complexity of
600 branching/ramified processes) that could be relevant in response to ethanol. Regarding the
601 literature, only a previous study described an effect of cannabinoid activation (cannabidiol
602 and Δ^9-THC) on amoeboid versus branched phenotypes of mouse microglial cell line BV-2
603 (McHugh et al., 2014).
604
605 **4.3. URB597 effects on cognitive and memory function**
606 The endocannabinoid system is a key regulator of memory consolidation for aversive
607 experiences (Morena and Campologno, 2014). In this regard, URB597 was described to
608 facilitate memory consolidation through a concurrent activation of both CB1 and CB2
609 receptors within prefrontal-limbic circuits (Morena et al., 2014). Moreover, accumulated
610 evidence indicate an association between neuroinflammation and cognitive impairment, a
611 relationship that can be likely mediated by the immunomodulatory effect of CB2 receptor
612 controlling microglial activity (Sun et al., 2017) and neuroprotection by preventing neuronal
613 apoptosis and improving cognition via PI3K/AKT signaling (Su et al., 2016). The current
614 study assessed the association among cannabinoid activation, neuroinflammation and memory
615 improvement despite ethanol exposure.
616
617 **4.4. Conclusions**

618 These findings indicate that increased *N*-acylethanolamine signaling (AEA, OEA) through
619 inhibition of its metabolizing enzyme FAAH by URB597 modulates microglial morphology
620 and phenotyping (cytokines and chemokines) via innate immune TLR4 signaling that may be
621 effectively associated with ethanol-related neuroinflammatory activity and an improved
622 hippocampal-dependent memory despite ethanol exposure.

623

624 **5. REFERENCES**

625 Afshar M, Richards S, Mann D, Cross A, Smith GB, Netzer G, Kovacs E, Hasday J. Acute
626 immunomodulatory effects of binge alcohol ingestion. Alcohol. 2015 Feb;49(1):57-64.
627 doi: 10.1016/j.alcohol.2014.10.002.

628 Antón M, Alén F, Gómez de Heras R, Serrano A, Pavón FJ, Leza JC, García-Bueno B,
629 Rodríguez de Fonseca F, Orio L. Oleoylethanolamide prevents neuroimmune
630 HMGB1/TLR4/NF-kB danger signaling in rat frontal cortex and depressive-like
631 behavior induced by ethanol binge administration. Addict Biol. 2017 May;22(3):724-
632 741. doi: 10.1111/adb.12365.

633 Ativie F, Albayram O, Bach K, Pradier B, Zimmer A, Bilkei-Gorzo A. Enhanced microglial
634 activity in FAAH(-/-) animals. Life Sci. 2015 Oct 1;138:52-6. doi:
635 10.1016/j.lfs.2014.12.016.

636 Bilbao A, Serrano A, Cippitelli A, Pavón FJ, Giuffrida A, Suárez J, García-Marchena N,
637 Baixeras E, Gómez de Heras R, Orio L, Alén F, Ciccocioppo R, Cravatt BF, Parsons
638 LH, Piomelli D, Rodríguez de Fonseca F. Role of the satiety factor
639 oleoylethanolamide in alcoholism. Addict Biol. 2016 Jul;21(4):859-72. doi:
640 10.1111/adb.12276.

641 Blednov YA, Bergeson SE, Walker D, Ferreira VM, Kuziel WA, Harris RA. Perturbation of
642 chemokine networks by gene deletion alters the reinforcing actions of ethanol. Behav
643 Brain Res. 2005 Nov 30;165(1):110-25.

644 Broadwater MA, Liu W, Crews FT, Spear LP. Persistent loss of hippocampal neurogenesis
645 and increased cell death following adolescent, but not adult, chronic ethanol exposure.
646 Dev Neurosci. 2014;36(3-4):297-305. doi: 10.1159/000362874.

647 Chung WS, Allen NJ, Eroglu C. Astrocytes control synapse formation, function, and
648 elimination. Cold Spring Harb Perspect Biol. 2015 Feb 6;7(9):a020370. doi:
649 10.1101/cshperspect.a020370.
650 Crews FT, Bechara R, Brown LA, Guidot DM, Mandrekar P, Oak S, Qin L, Szabo G,
651 Wheeler M, Zou J. Cytokines and alcohol. Alcohol Clin Exp Res. 2006
652 Apr;30(4):720-30.
653 Crews FT, Sarkar DK, Qin L, Zou J, Boyadjieva N, Vetreno RP. Neuroimmune function and
654 the consequences of alcohol exposure. Alcohol Res. 2015;37(2):331-41, 344-51.
655 Crews FT, Vetreno RP. Mechanisms of neuroimmune gene induction in alcoholism.
656 Psychopharmacology (Berl). 2016 May;233(9):1543-57. doi: 10.1007/s00213-015-
657 3906-1.
658 Cruz C, Meireles M, Silva SM. Chronic ethanol intake induces partial microglial activation
659 that is not reversed by long-term ethanol withdrawal in the rat hippocampal formation.
660 Neurotoxicology. 2017 May;60:107-115. doi: 10.1016/j.neuro.2017.04.005.
661 Cui C, Grandison L, Noronha A. Neuroimmune mechanisms of brain function and alcohol
662 related disorders. Brain Behav Immun. 2011 Jun;25 Suppl 1:S1-3. doi:
663 10.1016/j.bbi.2011.03.005.
664 De Bellis MD, Clark DB, Beers SR, Soloff PH, Boring AM, Hall J, Kersh A, Keshavan MS.
665 Hippocampal volume in adolescent-onset alcohol use disorders. Am J Psychiatry.
666 2000 May;157(5):737-44.
667 De Bellis MD, Narasimhan A, Thatcher DL, Keshavan MS, Soloff P, Clark DB. Prefrontal
668 cortex, thalamus, and cerebellar volumes in adolescents and young adults with
669 adolescent-onset alcohol use disorders and comorbid mental disorders. Alcohol Clin
670 Exp Res. 2005 Sep;29(9):1590-600.
671 Eggen BJ, Raj D, Hanisch UK, Boddeke HW. Microglial phenotype and adaptation. J
672 Neuroimmune Pharmacol. 2013 Sep;8(4):807-23. doi: 10.1007/s11481-013-9490-4.
673 Ehrhart J, Obregon D, Mori T, Hou H, Sun N, Bai Y, Klein T, Fernandez F, Tan J, Shytle RD.
674 Stimulation of cannabinoid receptor 2 (CB2) suppresses microglial activation. J
675 Neuroinflammation. 2005 Dec 12;2:29.
676 Ennaceur A, Delacour J. A new one-trial test for neurobiological studies of memory in rats. 1:
677 Behavioral data. Behav Brain Res. 1988 Nov 1;31(1):47-59.
678 Fernández-Arjona MDM, Grondona JM, Granados-Durán P, Fernández-Llebrez P, López-
679 Ávalos MD. Microglia morphological categorization in a rat model of

680 neuroinflammation by hierarchical cluster and principal components analysis. Front
681 Cell Neurosci. 2017 Aug 8;11:235. doi: 10.3389/fncel.2017.00235.
682 Fernández-López D, Faustino J, Derugin N, Wendland M, Lizasoain I, Moro MA, Vexler ZS.
683 Reduced infarct size and accumulation of microglia in rats treated with WIN 55,212-2
684 after neonatal stroke. Neuroscience. 2012 Apr 5;207:307-15. doi:
685 10.1016/j.neuroscience.2012.01.008.
686 Fernández-Ruiz J, Gómez-Ruiz M, García C, Hernández M, Ramos JA. Modeling
687 neurodegenerative disorders for developing cannabinoid-based neuroprotective
688 therapies. Methods Enzymol. 2017;593:175-198. doi: 10.1016/bs.mie.2017.06.021.
689 García-Marchena N, Araos PF, Barrios V, Sánchez-Marín L, Chowen JA, Pedraz M, Castilla-
690 Ortega E, Romero-Sanchiz P, Ponce G, Gavito AL, Decara J, Silva D, Torrens M,
691 Argente J, Rubio G, Serrano A, de Fonseca FR, Pavón FJ. Plasma Chemokines in
692 patients with alcohol use disorders: association of CCL11 (Eotaxin-1) with psychiatric
693 comorbidity. Front Psychiatry. 2017 Jan 18;7:214. doi: 10.3389/fpsyt.2016.00214.
694 Guerri C, Pascual M. Mechanisms involved in the neurotoxic, cognitive, and neurobehavioral
695 effects of alcohol consumption during adolescence. Alcohol. 2010 Feb;44(1):15-26.
696 doi: 10.1016/j.alcohol.2009.10.003.
697 Hagemeyer N, Hanft KM, Akriditou MA, Unger N, Park ES, Stanley ER, Staszewski O,
698 Dimou L, Prinz M. Microglia contribute to normal myelinogenesis and to
699 oligodendrocyte progenitor maintenance during adulthood. Acta Neuropathol. 2017
700 Sep;134(3):441-458. doi: 10.1007/s00401-017-1747-1.
701 Harper C. The neuropathology of alcohol-specific brain damage, or does alcohol damage the
702 brain? J Neuropathol Exp Neurol. 1998 Feb;57(2):101-10.
703 He J, Crews FT. Increased MCP-1 and microglia in various regions of the human alcoholic
704 brain. Exp Neurol. 2008 Apr;210(2):349-58. doi: 10.1016/j.expneurol.2007.11.017.
705 Kane CJ, Phelan KD, Douglas JC, Wagoner G, Johnson JW, Xu J, Phelan PS, Drew PD.
706 Effects of ethanol on immune response in the brain: region-specific changes in
707 adolescent versus adult mice. Alcohol Clin Exp Res. 2014 Feb;38(2):384-91. doi:
708 10.1111/acer.12244.
709 Karperien A, Ahammer H, Jelinek HF. Quantitating the subtleties of microglial morphology
710 with fractal analysis. Front Cell Neurosci. 2013 Jan 30;7:3. doi:
711 10.3389/fncel.2013.00003.
712 Langballe EM, Ask H, Holmen J, Stordal E, Saltvedt I, Selbæk G, Fikseaunet A, Bergh S,
713 Nafstad P, Tambs K. Alcohol consumption and risk of dementia up to 27 years later in

714 a large, population-based sample: the HUNT study, Norway. Eur J Epidemiol. 2015
715 Sep;30(9):1049-56. doi: 10.1007/s10654-015-0029-2.
716 López-Caneda E, Cadaveira F, Crego A, Doallo S, Corral M, Gómez-Suárez A, Rodríguez
717 Holguín S. Effects of a persistent binge drinking pattern of alcohol consumption in
718 young people: a follow-up study using event-related potentials. Alcohol Alcohol. 2013
719 Jul-Aug;48(4):464-71. doi: 10.1093/alcalc/agt046.
720 Marshall SA, McClain JA, Kelso ML, Hopkins DM, Pauly JR, Nixon K. Microglial activation
721 is not equivalent to neuroinflammation in alcohol-induced neurodegeneration: The
722 importance of microglia phenotype. Neurobiol Dis. 2013 Jun;54:239-51. doi:
723 10.1016/j.nbd.2012.12.016.
724 McHugh D, Roskowski D, Xie S, Bradshaw HB. Δ(9)-THC and N-arachidonoyl glycine
725 regulate BV-2 microglial morphology and cytokine release plasticity: implications for
726 signaling at GPR18. Front Pharmacol. 2014 Jan 2;4:162. doi:
727 10.3389/fphar.2013.00162.
728 Montesinos J, Alfonso-Loeches S, Guerri C. Impact of the innate immune response in the
729 actions of ethanol on the central nervous system. Alcohol Clin Exp Res. 2016
730 Nov;40(11):2260-2270. doi: 10.1111/acer.13208.
731 Montesinos J, Pascual M, Pla A, Maldonado C, Rodríguez-Arias M, Miñarro J, Guerri C.
732 TLR4 elimination prevents synaptic and myelin alterations and long-term cognitive
733 dysfunctions in adolescent mice with intermittent ethanol treatment. Brain Behav
734 Immun. 2015 Mar;45:233-44. doi: 10.1016/j.bbi.2014.11.015.
735 Morena M, Campolongo P. The endocannabinoid system: an emotional buffer in the
736 modulation of memory function. Neurobiol Learn Mem. 2014 Jul;112:30-43. doi:
737 10.1016/j.nlm.2013.12.010.
738 Morena M, Roozendaal B, Trezza V, Ratano P, Peloso A, Hauer D, Atsak P, Trabace L,
739 Cuomo V, McGaugh JL, Schelling G, Campolongo P. Endogenous cannabinoid
740 release within prefrontal-limbic pathways affects memory consolidation of emotional
741 training. Proc Natl Acad Sci U S A. 2014 Dec 23;111(51):18333-8. doi:
742 10.1073/pnas.1420285111.
743 Murphy N, Cowley TR, Blau CW, Dempsey CN, Noonan J, Gowran A, Tanveer R, Olango
744 WM, Finn DP, Campbell VA, Lynch MA. The fatty acid amide hydrolase inhibitor
745 URB597 exerts anti-inflammatory effects in hippocampus of aged rats and restores an
746 age-related deficit in long-term potentiation. J Neuroinflammation. 2012 Apr 26;9:79.
747 doi: 10.1186/1742-2094-9-79.

748 Nimmerjahn A, Kirchhoff F, Helmchen F. Resting microglial cells are highly dynamic
749 surveillants of brain parenchyma in vivo. Science. 2005 May 27;308(5726):1314-8.
750 Palazuelos J, Davoust N, Julien B, Hatterer E, Aguado T, Mechoulam R, Benito C, Romero J,
751 Silva A, Guzmán M, Nataf S, Galve-Roperh I. The CB(2) cannabinoid receptor
752 controls myeloid progenitor trafficking: involvement in the pathogenesis of an animal
753 model of multiple sclerosis. J Biol Chem. 2008 May 9;283(19):13320-9. doi:
754 10.1074/jbc.M707960200.
755 Parada M, Corral M, Caamaño-Isorna F, Mota N, Crego A, Holguín SR, Cadaveira F. Binge
756 drinking and declarative memory in university students. Alcohol Clin Exp Res. 2011
757 Aug;35(8):1475-84. doi: 10.1111/j.1530-0277.2011.01484.x.
758 Pascual M, Montesinos J, Guerri C. Role of the innate immune system in the
759 neuropathological consequences induced by adolescent binge drinking. J Neurosci
760 Res. 2018 May;96(5):765-780. doi: 10.1002/jnr.24203.
761 Pascual M, Montesinos J, Montagud-Romero S, Forteza J, Rodríguez-Arias M, Miñarro J,
762 Guerri C. TLR4 response mediates ethanol-induced neurodevelopment alterations in a
763 model of fetal alcohol spectrum disorders. J Neuroinflammation. 2017 Jul
764 24;14(1):145. doi: 10.1186/s12974-017-0918-2.
765 Paxinos G, Watson C. The Rat Brain in Stereotaxic Coordinates, 6th Edn. 2007. Sidney:
766 Academic Press.
767 Pezze MA, Marshall HJ, Fone KC, Cassaday HJ. Dopamine D1 receptor stimulation
768 modulates the formation and retrieval of novel object recognition memory: Role of the
769 prelimbic cortex. Eur Neuropsychopharmacol. 2015 Nov;25(11):2145-56. doi:
770 10.1016/j.euroneuro.2015.07.018.
771 Pfefferbaum A, Sullivan EV, Hedehus M, Adalsteinsson E, Lim KO, Moseley M. In vivo
772 detection and functional correlates of white matter microstructural disruption in
773 chronic alcoholism. Alcohol Clin Exp Res. 2000 Aug;24(8):1214-21.
774 Pradier B, Erxlebe E, Markert A, Rácz I. Microglial IL-1β progressively increases with
775 duration of alcohol consumption. Naunyn Schmiedebergs Arch Pharmacol. 2018
776 Apr;391(4):455-461. doi: 10.1007/s00210-018-1475-7.
777 Qin L, Crews FT. Chronic ethanol increases systemic TLR3 agonist-induced
778 neuroinflammation and neurodegeneration. J Neuroinflammation. 2012 Jun 18;9:130.
779 doi: 10.1186/1742-2094-9-130.

780 Ramirez SH, Reichenbach NL, Fan S, Rom S, Merkel SF, Wang X, Ho WZ, Persidsky Y.
781 Attenuation of HIV-1 replication in macrophages by cannabinoid receptor 2 agonists. J
782 Leukoc Biol. 2013 May;93(5):801-10. doi: 10.1189/jlb.1012523.
783 Ratano P, Petrella C, Forti F, Passeri PP, Morena M, Palmery M, Trezza V, Severini C,
784 Campolongo P. Pharmacological inhibiton of 2-arachidonoilglycerol hydrolysis
785 enhances memory consolidation in rats through CB2 receptor activation and mTOR
786 signaling modulation. Neuropharmacology. 2018 May 26. doi:
787 10.1016/j.neuropharm.2018.05.030.
788 Rivera P, Bindila L, Pastor A, Pérez-Martín M, Pavón FJ, Serrano A, de la Torre R, Lutz B,
789 Rodríguez de Fonseca F, Suárez J. Pharmacological blockade of the fatty acid amide
790 hydrolase (FAAH) alters neural proliferation, apoptosis and gliosis in the rat
791 hippocampus, hypothalamus and striatum in a negative energy context. Front Cell
792 Neurosci. 2015 Mar 27;9:98. doi: 10.3389/fncel.2015.00098.
793 Rivera P, Blanco E, Bindila L, Alen F, Vargas A, Rubio L, Pavón FJ, Serrano A, Lutz B,
794 Rodríguez de Fonseca F, Suárez J. Pharmacological activation of CB2 receptors
795 counteracts the deleterious effect of ethanol on cell proliferation in the main
796 neurogenic zones of the adult rat brain. Front Cell Neurosci. 2015 Sep 29;9:379. doi:
797 10.3389/fncel.2015.00379.
798 Roche M, Kelly JP, O'Driscoll M, Finn DP. Augmentation of endogenous cannabinoid tone
799 modulates lipopolysaccharide-induced alterations in circulating cytokine levels in rats.
800 Immunology. 2008 Oct;125(2):263-71. doi: 10.1111/j.1365-2567.2008.02838.x.
801 Rom S, Persidsky Y. Cannabinoid receptor 2: potential role in immunomodulation and
802 neuroinflammation. J Neuroimmune Pharmacol. 2013 Jun;8(3):608-20. doi:
803 10.1007/s11481-013-9445-9.
804 Sánchez AJ, García-Merino A. Neuroprotective agents: cannabinoids. Clin Immunol. 2012
805 Jan;142(1):57-67. doi: 10.1016/j.clim.2011.02.010.
806 Sanchez-Marin L, Pavon FJ, Decara J, Suarez J, Gavito A, Castilla-Ortega E, Rodriguez de
807 Fonseca F, Serrano A. Effects of intermittent alcohol exposure on emotion and
808 cognition: a potential role for the endogenous cannabinoid system and
809 neuroinflammation. Front Behav Neurosci. 2017 Feb 7;11:15. doi:
810 10.3389/fnbeh.2017.00015.
811 Schafer DP, Stevens B. Microglia function in central nervous system development and
812 plasticity. Cold Spring Harb Perspect Biol. 2015 Jul 17;7(10):a020545. doi:
813 10.1101/cshperspect.a020545.

814 Serrano A, Rivera P, Pavon FJ, Decara J, Suárez J, Rodriguez de Fonseca F, Parsons LH.
815 Differential effects of single versus repeated alcohol withdrawal on the expression of
816 endocannabinoid system-related genes in the rat amygdala. Alcohol Clin Exp Res.
817 2012 Jun;36(6):984-94. doi: 10.1111/j.1530-0277.2011.01686.x.
818 Soltys Z, Orzylowska-Sliwinska O, Zaremba M, Orlowski D, Piechota M, Fiedorowicz A,
819 Janeczko K, Oderfeld-Nowak B. Quantitative morphological study of microglial cells
820 in the ischemic rat brain using principal component analysis. J Neurosci Methods.
821 2005 Jul 15;146(1):50-60.
822 Spear LP. Consequences of adolescent use of alcohol and other drugs: Studies using rodent
823 models. Neurosci Biobehav Rev. 2016 Nov;70:228-243. doi:
824 10.1016/j.neubiorev.2016.07.026.
825 Stella N. Endocannabinoid signaling in microglial cells. Neuropharmacology. 2009;56 Suppl
826 1:244-53. doi: 10.1016/j.neuropharm.2008.07.037.
827 Stellwagen D, Malenka RC. Synaptic scaling mediated by glial TNF-alpha. Nature. 2006 Apr
828 20;440(7087):1054-9.
829 Su SH, Wang YQ, Wu YF, Wang DP, Lin Q, Hai J. Cannabinoid receptor agonist
830 WIN55,212-2 and fatty acid amide hydrolase inhibitor URB597 may protect against
831 cognitive impairment in rats of chronic cerebral hypoperfusion via PI3K/AKT
832 signaling. Behav Brain Res. 2016 Oct 15;313:334-44. doi: 10.1016/j.bbr.2016.07.009.
833 Sun L, Dong R, Xu X, Yang X, Peng M. Activation of cannabinoid receptor type 2 attenuates
834 surgery-induced cognitive impairment in mice through anti-inflammatory activity. J
835 Neuroinflammation. 2017 Jul 19;14(1):138. doi: 10.1186/s12974-017-0913-7.
836 Szabo G, Saha B. Alcohol's Effect on Host Defense. Alcohol Res. 2015;37(2):159-70.
837 Tang J, Miao H, Jiang B, Chen Q, Tan L, Tao Y, Zhang J, Gao F, Feng H, Zhu G, Chen Z. A
838 selective CB2R agonist (JWH133) restores neuronal circuit after Germinal Matrix
839 Hemorrhage in the preterm via CX3CR1(+) microglia. Neuropharmacology. 2017
840 Jun;119:157-169. doi: 10.1016/j.neuropharm.2017.01.027.
841 van Praag H, Schinder AF, Christie BR, Toni N, Palmer TD, Gage FH. Functional
842 neurogenesis in the adult hippocampus. Nature. 2002 Feb 28;415(6875):1030-4.
843

844

845

846

847 **6. LEGENDS TO FIGURES**

848 **Figure 1.** Effects of OEA (10 mg/kg), JWH133 (0.2 mg/kg), ACEA (3 mg/kg), AEA (10
849 mg/kg) and URB597 (0.3 mg/kg) i.p. administrations during the last 5 days of ethanol
850 exposure (10%) for 2 weeks on IBA-1-immunoreactive microglial cells in the dentate gyrus
851 (DG) (**A**), CA3 (**B**) and CA1 (**C**) hippocampal areas, and the whole hippocampus (**D**). The
852 histograms represent the mean + SEM per area (mm^2) (n = 6 rats per experimental group).
853 Tukey's test: */**/***P<0.05/0.01/0.001 *vs*. sucrose-vehicle group; $^{\#/\#\#/\#\#\#}P$<0.05/0.01/0.001
854 *vs*. ethanol-vehicle group. Representative microphotographs showing magnification views of
855 the immunostaining in hippocampus (**E-P**). Scale bars are included in E image.

856

857 **Figure 2.** Effects of OEA, JWH133, ACEA, AEA and URB597 i.p. administrations during
858 the last 5 days of ethanol exposure (10%) for 2 weeks on morphometric parameter such as *cell*
859 *area* (**A**), *cell perimeter* (**B**), *density* (**C**), *roughness* (**D**), *fractal dimension* (**E**) and *lacunarity*
860 (**F**) in microglial cells of the DG. Representative microphotographs showing high
861 magnification views of the microglial morphology can be observed in Figure S1. Results of
862 additional morphometric parameters can be found in Figure S2. The histograms represent the
863 mean + SEM (n = 50 cells per experimental group). Kruskal-Wallis test: */***P<0.05/0.001
864 *vs*. vehicle group; $^{\#\#\#}P$<0.001 *vs*. sucrose-exposed rats with the same treatment.

865

866 **Figure 3.** Effects of OEA, JWH133, ACEA, AEA and URB597 i.p. administrations during
867 the last 5 days of ethanol exposure (10%) for 2 weeks on iNOS-immunoreactive microglial
868 cells in the DG (**A**), CA3 (**B**) and CA1 (**C**) hippocampal areas, and the whole hippocampus
869 (**D**). The histograms represent the mean + SEM per area (mm^2) (n = 6 rats per experimental
870 group). Tukey's test: */**/***P<0.05/0.01/0.001 *vs*. sucrose-vehicle group; $^{\#/\#\#}P$<0.05/0.01

871 *vs*. ethanol-vehicle group. Representative microphotographs showing magnification views of
872 the immunostaining in DG (**E-P**). Scale bars are included in E image.
873
874 **Figure 4.** Effects of OEA, JWH133, ACEA, AEA and URB597 i.p. administrations during
875 the last 5 days of ethanol exposure (10%) for 2 weeks on GFAP-immunoreactive astroglial
876 cells in the DG (**A**), CA3 (**B**) and CA1 (**C**) hippocampal areas, and the whole hippocampus
877 (**D**). The histograms represent the mean + SEM per area (mm^2) (n = 6 rats per experimental
878 group). Tukey's test: */**/****P*<0.05/0.01/0.001 *vs*. sucrose-vehicle group;
879 $^{\#\#/\#\#\#}P$<0.01/0.001 *vs*. ethanol-vehicle group. Representative microphotographs showing
880 magnification views of the immunostaining in DG (**E-P**). Scale bars are included in E image.
881
882 **Figure 5.** Effects of URB597 i.p. administration during the last 5 days of ethanol exposure
883 (10%) for 2 weeks on mRNA levels of *Iba1*, *Tnfα*, *IL-1β*, *IL-6* and *TLR4* (**A**), as well as *Gfap*,
884 *SDF-1α*, *MCP-1*, *eotaxin-1* and *fractalkine* (**B**) in the hippocampus. The histograms represent
885 the mean + SEM per area (mm^2) (n = 6 rats per experimental group). Tukey's test:
886 */****P*<0.05/0.001 *vs*. sucrose-vehicle group; $^{\#/\#\#/\#\#\#}P$<0.05/0.01/0.001 *vs*. ethanol-vehicle
887 group.
888
889 **Figure 6.** Effects of URB597 i.p. administration during the last 5 days of ethanol exposure
890 (10%) for 2 weeks on cells expressing the chemokine receptors CX3CR1 (**A**), CCR2 (**B**),
891 CCR4 (**C**) and CXCR4 (**D**) in the DG, CA3 and CA1 hippocampal areas, and the whole
892 hippocampus. The histograms represent the mean + SEM per area (mm^2) (n = 6 rats per
893 experimental group). Tukey's test: */**/****P*<0.05/0.01/0.001 *vs*. sucrose-vehicle group;
894 $^{\#\#/\#\#\#}P$<0.01/0.001 *vs*. ethanol-vehicle group; $^{\$\$}p$<0.01 vs URB597-treated, sucrose-exposed

895 rats. Representative microphotographs showing magnification views of the immunostaining
896 for CX3CR1 (**E**), CCR2 (**F**), CCR4 (**G**) and CXCR4 (**H**). Scale bars are included in E image.
897
898 **Figure 7.** Effects of URB597 i.p. administration during the last 5 days of ethanol exposure
899 (10%) for 2 weeks on discrimination index [N/(N+F)] of distance, duration, frequency and
900 duration/frequency ratio obtained from short-term (**A**) and long-term (**B**) object recognition
901 (OR) tests (recognition memory). The histograms represent the mean + SEM per area (mm^2)
902 (*n* = 6 rats per experimental group). Tukey's test: */****P*<0.05/0.001 *vs*. sucrose-vehicle
903 group; $^{\#}P$<0.05 *vs*. ethanol-vehicle group.
904
905 **Figure S1**. Pre-processing of cell digital image. After random selection of DG microglial
906 cells from each experimental condition (**A**), the images were filtered, changed to grayscale
907 and transformed into a binary image. We finally obtained a filled shape and its pairwise
908 outline shape (**B**) to be used for morphological parameters measures (**C**).
909
910 **Figure S2**. Effects of OEA, JWH133, ACEA, AEA and URB597 i.p. administrations during
911 the last 5 days of ethanol exposure (10%) for 2 weeks on additional morphometric parameter
912 such as *convex hull area* (**A**), *convex hull perimeter* (**B**), *maximum span across the convex*
913 *hull* (**C**), *convex hull span ratio* (**D**), *diameter of the bounding circle* (**E**), *cell circularity* (**F**),
914 *the maximum mass center radius* (**G**), *the ratio maximum/minimum convex hull radii* (**H**), and
915 *the mean radius* (**I**) in microglial cells of the DG. Representative microphotographs showing
916 high magnification views of the microglial morphology can be observed in Figure S1. The
917 histograms represent the mean + SEM (*n* = 50 cells per experimental group).
918
919

920 **Table S1.** List of primers used to perform PCR analysis from TaqMan® Gene Expression

921 Assays (ThermoFisher).

Gen name[1]	Gen code	Amplicon length
Gadph	Rn01775763_g1	174
Gfap	Rn01253033_m1	75
Iba1/Aif1	Rn00574125_g1	126
IL-1β	Rn00580432_m1	74
Il-6	Rn01410330_m1	121
Tnfα	Rn01525859_g1	92
TLR4	Rn00569848_m1	127
Eotaxin-1/CCL11	Rn00569995_m1	75
Fractalkine/CX3CL1	Rn00593186_m1	74
MCP-1/Ccl2	Rn00580555_m1	95
SDF-1a/CXCL12	Rn00573260_m1	60

922 [1]Abbreviations: *Gadph*, Glyceraldehyde 3-phosphate dehydrogenase; *Gfap*, Glial fibrillary

923 acidic protein; *Iba1*, ionized calcium-binding adapter molecule 1; *IL-1β*, interleukin 1 beta;

924 *IL-6*, interleukin 6; *Tnfα*, tumor necrosis factor alpha; *TLR4*, toll-like receptor 4; *eotaxin-*

925 *1/CCL11*, eosinophil chemotactic protein (C-C motif chemokine 11); *fractalkine/CX3CL1*,

926 chemokine (C-X3-C motif) ligand 1; *MCP-1/CCL2*, monocyte chemoattractant protein 1

927 (chemokine (C-C motif) ligand 2); *SDF-1α/CXCL12*, stromal cell-derived factor 1 (C-X-C

928 motif chemokine 12).